24

Thermal Energy Storage Tanks Using Phase Change Material (PCM) in HVAC Systems

Motoi Yamaha[1] and Nobuo Nakahara[2]
[1]*Chubu University,*
[2]*Nakahara Laboratory, Environmental Syst.-Tech.*
Japan

1. Introduction

Thermal energy storage (TES) systems, which store energy as heat, can compensate for energy imbalances between heat generation and consumption (Tamblyn, 1977). Thermal energy storage systems designed for use with solar energy can accumulate unstable solar insolation. These systems can also shave the peak heat demand to off-peak hours. As such, the required capacity of refrigeration machines can be reduced by extending the time during which these machines are operated. These system also offer other advantages, such as load leveling for the energy supply side. Electric utility companies in Japan offer discount rates during nighttime to promote peak shaving.

Methods of storing heat can be classified as sensible, latent, or chemical storage methods. Sensible heat storage uses heat capacity obtained through a temperature difference. Latent heat storage utilizes the heat to produce a phase change. Considering the associated volume expansion, the phase change between a liquid and a solid is generally used. Reversible chemical thermal reactions can also be used to store heat.

For latent heat storage, various phase change materials (PCM) for different temperature ranges have been investigated. Since these materials should be inexpensive, abundant, and safe, water or ice are the most attractive storage materials for use in the heating, ventilation, and air conditioning (HVAC) field. Water has a relatively high heat of fusion and a melting temperature that is suitable for cooling. The freezing point is suitable for comfort cooling, even though the low evaporation temperature of the refrigeration cycle decreases the efficiency of the machine. Since the tank volume is smaller than the water tank, heat losses from the tank are also smaller. Buildings that do not have sufficient space for water storage still can take advantage of TES through the use of ice storage tanks.

Although ice storage tanks have been used successfully in commercial applications, their use is limited to cooling applications and lowers the efficiency of refrigeration machines due to the lower evaporative temperature associated with these tanks. Phase change materials other than ice have been studied for various purposes. Paraffin waxes, salt hydrates, and eutectic mixtures are materials for use in building applications. Compared to ice storage, these PCMs are used in a passive manner such as the stabilization of room temperature by means of the thermal inertia of phase change.

In this chapter, performance indices are discussed for ice storage and an estimation method is demonstrated experimentally. Furthermore, PCM storage using paraffin waxes in a passive method is evaluated.

2. Analysis of performance of ice thermal storage in HAVC systems

Ice thermal storage is the most common type of latent heat storage. Although a large number of applications exist in countries with warm climates, the performance of ice thermal storage in HVAC systems has not been analyzed. Since the heat of fusion of water is relatively large, the performance of ice thermal storage is usually evaluated from the viewpoint of the amount of heat. However, the temperature response at the outlet of the ice storage tank should be considered if the transient status of the entire HVAC system is discussed.

Ice storage systems can be classified as static systems, in which ice is fixed around a heat exchanger, or slurry ice systems, in which ice floats inside the storage tank. In the following sections, definitions of efficiency are presented, and the effect on the efficiency of the conditions at the inlet for both types is analyzed experimentally.

2.1 Definitions of efficiency for evaluating tanks

Efficiencies should be defined when evaluating the performance of storage tanks. Therefore, the present author has proposed several definitions of efficiencies:

2.2 Response-based efficiency η

A tank is modeled as shown in Figure 1. The heat removed from the tank (Ht) until time T can be calculated according to the following equation, when a step input of temperature θ_{in} and flow rate Q is assumed.

$$Ht = \rho c Q \int_0^T (\theta_{in} - \theta_{out}) dt \tag{1}$$

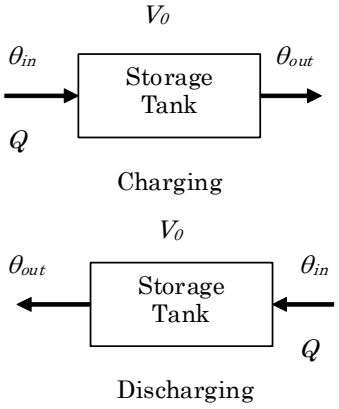

Fig. 1. Model of a tank

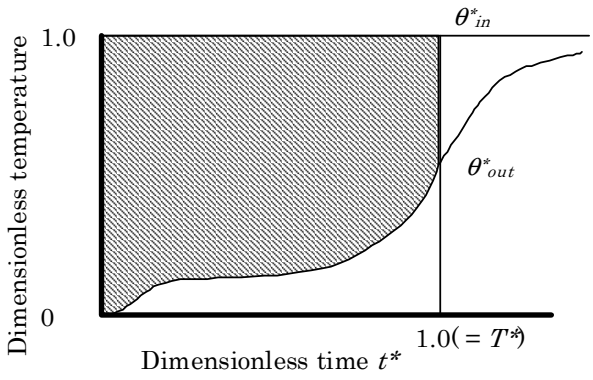

Fig. 2. Response-based efficiency η

Since θ_{in} is constant, the heat discharged until the water in the tank is completely changed ($T = Vo/Q$) is calculated as follows:

$$Ht = \rho c Q \left[\theta_{in} T - \int_0^T \theta_{out} dt \right] \tag{2}$$

The above equation is normalized by the following dimensionless variables:

$$\theta_{out}^* = \frac{\theta_{out} - \theta_0}{\theta_{in} - \theta_0} \tag{3}$$

$$t^* = \frac{Q}{V_0} t \tag{4}$$

Substituting these variables and considering that $T^* = 1$, the following equation is obtained:

$$\frac{Ht}{\rho c(\theta_{in} - \theta_0) V_0} = 1 - \int_0^1 \theta_{out}^* dt^* \tag{5}$$

The left-hand side of Equation (5) represents the ratio of discharged heat to possible heat to be stored. The efficiency, which can be obtained from the dimensionless response, is indicated by the hatched area in Figure 2.

2.2.1 System efficiency η_0

In actual applications, the outlet water from a storage tank is supplied to secondary systems, i.e., air handling units. The temperature of the water is raised by a certain temperature difference by exchanging heat at the coils of the air handling units, and the water is then returned to the tank. Although the heat from the tank can be calculated using Equation (5), in this case, the inlet temperature varies. The heat is supplied until the outlet temperature of the storage reaches a specific temperature, which is higher than the temperature required

for cooling and dehumidification. This temperature is defined as the limit temperature (θ_c) of the coils of the air handling units. Assuming that the time is T_c when the outlet temperature reaches the limit temperature, if the temperature difference for discharge is constant as $\Delta\theta = \theta_{in} - \theta_{out}$, then Equation (6) can be rewritten as follows:

$$Ht_c = \rho c Q \Delta\theta T_c \tag{7}$$

which is normalized according to Equations (3) and (4) to obtain

$$\frac{H_{Tc}}{\rho c(\theta_{in} - \theta_0)V_0} = \frac{Q}{V_0} T_c = T_c^* \tag{8}$$

In Figure 3, the efficiency is represented by the hatched area between the inlet and outlet curves until the limit temperature is reached.

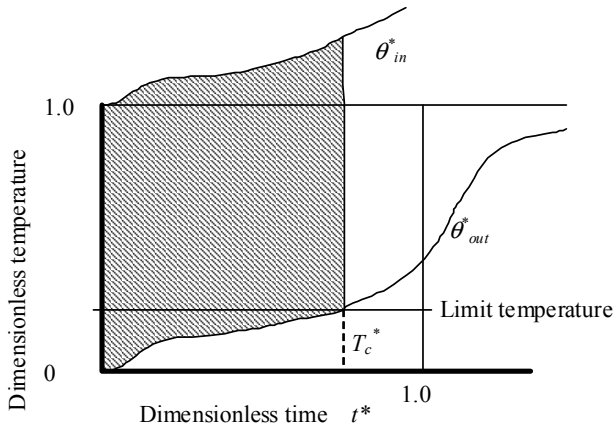

Fig. 3. System-based efficiency η_0

$$Ht_c = \rho c Q \int_0^{T_c} (\theta_{in} - \theta_{out}) dt \tag{6}$$

2.2.2 Volumetric efficiency η_v

Efficiency can also be defined based on the temperature profile. The heat obtained from the tank can therefore be indicated by the hatched area between the two curves on the left-hand side of Figure 4. The volumetric efficiency is defined as the ratio of the hatched area to the rectangular area. For an ice storage tank, an equivalent temperature difference ($\Delta\theta_i$), which is the quotient of the stored latent heat and specific heat of water, was introduced in order to represent the latent heat in terms of temperature. The volumetric efficiency is defined as follows:

$$\eta_v = \frac{H_t}{c\rho\Delta\theta_0 V_0} \tag{9}$$

Since $\Delta\theta_0$ in Equation (9) is the temperature difference at the coil of an air handling unit, the definition of efficiency can be adapted to both ice and water storage tanks. Since the value of $\eta_{v\_}$ can be greater than unity by definition, the excess can be considered to represent the reduction in tank volume due to ice storage by latent heat.

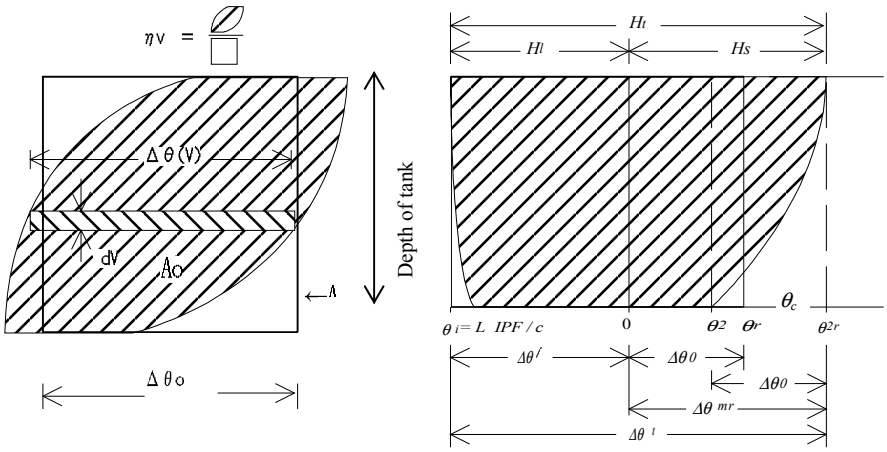

(a) water storage tank (b) ice storage tank

Fig. 4. Definition of tank volume efficiency

2.3 Thermal response of the ice-on-coil ice storage tank

2.3.1 Experimental setup and conditions

Figure 5 shows the experimental setup of an ice-on-coil ice storage tank. The input temperature could be maintained constant by conditioned water supplied from a hot water tank and a chilled water tank. The flow rate to the experimental tank was controlled by the difference in water level between a high tank and the experimental tank. The experimental tank consisted of transparent acrylic plates. The coil was constructed from polyethylene pipes, as shown in Figure 6. Temperature was measured by thermocouples and the quantity of ice was calculated by measuring the water level of the tank. The ice packing factor (IPF), which is the volumetric ratio of ice to water (V_{ice}/V_0), was calculated from the measured quantity of ice.

Factors for thermal response are chosen considering fluid dynamics and heat transfer. Reynolds number and Archimedes number are the dominant dimensionless numbers used in analyzing non-isothermal fluid flow, although experiments for water thermal storage tanks indicate that the Reynolds number is less influential. Therefore, the Archimedes number at the inlet of the tank, as defined by the following equation, is the dominant dimensionless number:

$$\mathrm{Ar}_{in} = \frac{d_{in} g(\Delta\rho/\rho_0)}{u_{in}^2} \tag{10}$$

Furthermore, the enthalpy flow at the inlet is also an important factor with respect to the thermal response of an ice storage tank. The dimensionless enthalpy flow rate is defined as follows:

$$Q^* = \frac{\rho c Q \theta_{in}}{\rho c V_0 \theta_{in} + \rho_{ice} V_0 IPF \cdot L} \tag{11}$$

The experimental conditions are listed in Tables 1 through 4.

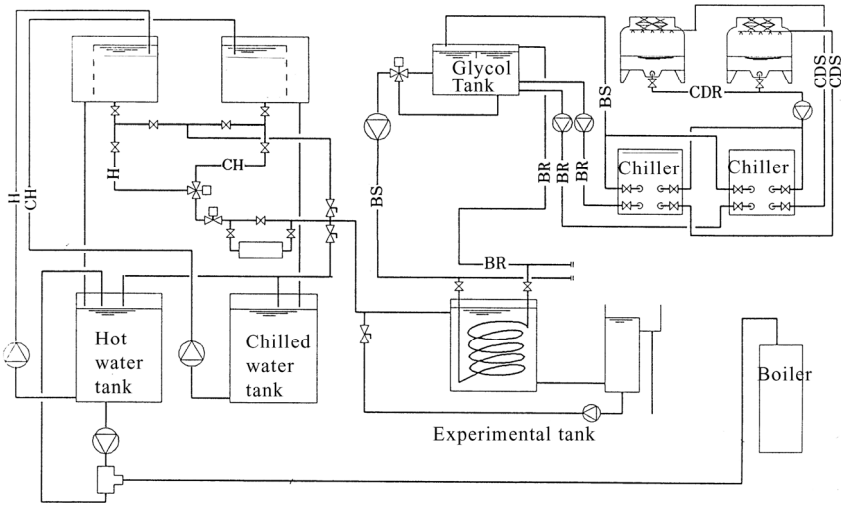

Fig. 5. Schematic diagram of the experimental setup

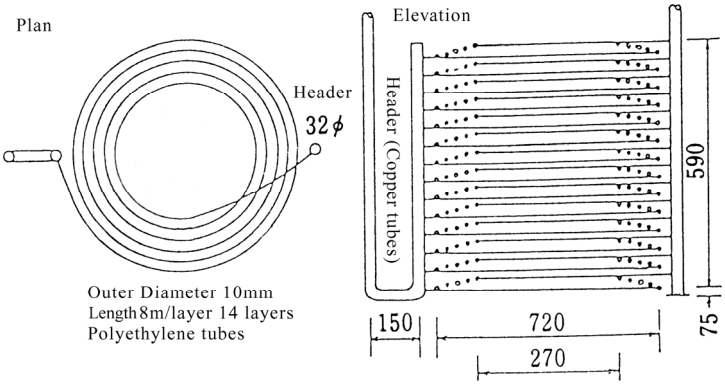

Fig. 6. Structure of the ice making coil

2.4 Results

Figure 7 shows the temperature response of the upper and lower parts of the tank during the freezing process. With the exception of the upper part of the coil, the temperature in the tank decreased uniformly. Soon after the temperature at the bottom of the tank reached 4°C, at which the density of water is maximum, the temperature of the upper part of the tank decreased quickly. When the temperature reached 0°C, ice first formed on the header of the

coils and then formed on the entire coils. The patterns for the ice making process were approximately the same throughout the experiments.

The dimensionless response of the outlet temperature during the melting process is shown in Figures 8 through 10 for various Archimedes numbers and enthalpy flow rates. For the results shown in Figure 8, the outlet temperature increased immediately after the discharge process began and remained lower than 4°C until all of the ice in the tank had melted. The upper part of the tank was warmed by the inlet water and stratification developed. As the inlet enthalpy flow rate was large enough to maintain stratification, melting occurred primarily beneath the stratification. Since the inlet water was cooled by the remaining ice as the water passed through the tank, the outlet water remained at a lower temperature. The results of experiments conducted using a smaller enthalpy flow rate are shown in Figure 9. The outlet temperature gradually increased to 4°C and remained constant. Once the inlet water entered the tank, the water was cooled by melting ice and was mixed due to buoyancy effects. Melting occurred uniformly in the tank, and the temperature was maintained at 4°C during melting. For both conditions, the thermal characteristics were the same as for a stratified water tank, after complete melting. In Figure 10, the outlet temperature exceeded 4°C immediately after the start of the experiment. Since the Archimedes number was small for this condition, the momentum of the entering water from the inlet exceeded the buoyancy force, and hence the inside of the tank was completely mixed. Comparison of dimensionless responses for the same conditions, with the exception of the IPF, showed no significant differences. The IPF, which represents the quantity of ice, determined the duration of ice melting. However, the IPF had little effect on the dimensionless response.

Based on the above results, the dominant factors affecting mixing inside the tank and the outlet response are the Archimedes number and the inlet enthalpy flow rate. The response pattern is determined by the Archimedes number, and the melting pattern is determined by the enthalpy flow rate.

Exp. no	Initial temp. [°C]	Charging time [hr:min]	IPF [%]
SA01-11-1	14.9	3:45	10
SA01-21-1	9.3	2:55	10
SA01-31-1	15.3	3:30	10
SA01-12-1	10.1	2:55	10
SA01-22-1	13.1	3:15	10
SA01-32-1	18.7	3:00	10
SA01-42-1	18.8	3:26	10
SA01-13-1	10.0	2:55	10
SA01-23-1	12.7	3:25	10
SA01-33-1	14.7	3:25	10
SA01-43-1	18.9	3:40	10

Table 1. Experimental conditions of the freezing process for the ice-on-coil ice storage tank with IPF 10%

Exp. no	Initial temp. [°C]	Charging time [hr:min]	IPF [%]
SA01-11-2	7.6	5:00	20
SA01-21-2	7.8	5:30	20
SA01-31-2	15.3	4:30	20
SA01-12-2	12.9	4:20	20
SA01-22-2	14.1	4:50	20
SA01-32-2	15.5	4:30	20
SA01-42-2	12.4	4:27	20
SA01-13-2	12.5	4:30	20
SA01-23-2	17.2	4:45	20
SA01-33-2	--	--	20
SA01-43-2	15.2	4:15	20

Table 2. Experimental conditions of the freezing process for the ice-on-coil ice storage tank with IPF 20%

Exp. no	Input temp. [°C]	Flow rate [L/min]	Ar_{in} [-]	Inlet heat [kW]
SA01-11-1	10.7	5.9	2.62E-02	4.4
SA01-21-1	12.7	5.1	7.18E-02	4.5
SA01-31-1	15.4	4.1	2.03E-01	4.4
SA01-12-1	14.7	11.4	2.24E-01	11.6
SA01-22-1	18.3	8.9	6.72E-02	11.4
SA01-32-1	25.3	8.1	1.77E-01	14.3
SA01-42-1	10.9	16.0	4.10E-03	12.2
SA01-13-1	14.7	35.7	2.10E-02	36.6
SA01-23-1	18.4	27.8	6.39E-02	35.6
SA01-33-1	24.3	20.7	2.23E-01	35.1
SA01-43-1	15.3	32.3	3.11E-03	34.4

Table 3. Experimental conditions of the melting process for the ice-on-coil ice storage tank with IPF 10%

Exp. no	Input temp. [°C]	Flow rate [L/min]	Ar_{in} [-]	Inlet heat [kW]
SA01-11-2	10.8	6.0	2.76E-02	4.5
SA01-21-2	13.0	5.0	7.83E-02	4.5
SA01-31-2	15.4	4.0	2.03E-01	4.3
SA01-12-2	14.5	11.3	2.16E-01	11.4
SA01-22-2	18.3	8.9	6.78E-02	11.4
SA01-32-2	25.2	7.9	1.85E-01	13.9
SA01-42-2	10.5	15.5	3.61E-03	11.4
SA01-13-2	14.7	35.8	2.08E-02	36.7
SA01-23-2	18.3	27.7	6.30E-02	35.2
SA01-33-2	24.5	20.8	2.27E-01	35.6
SA01-43-2	15.3	33.8	2.87E-03	36.0

Table 4. Experimental conditions of the melting process for the ice-on-coil ice storage tank with IPF 10%

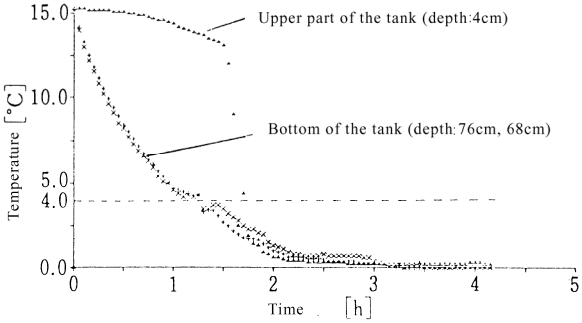

Fig. 7. Freezing process in the experiment using the ice-on-coil ice storage tank

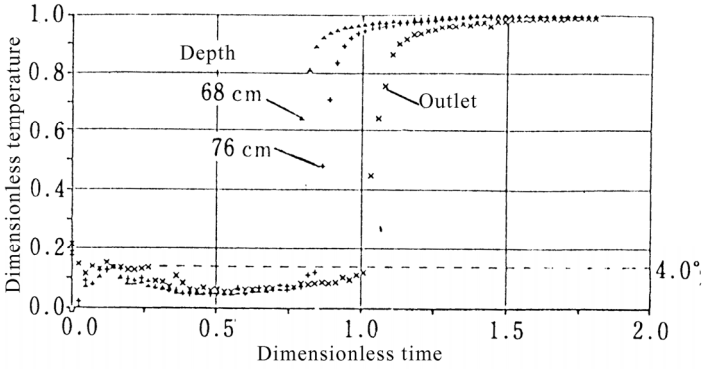

Fig. 8. Melting process for large Archimedes number and inlet enthalpy flow rate

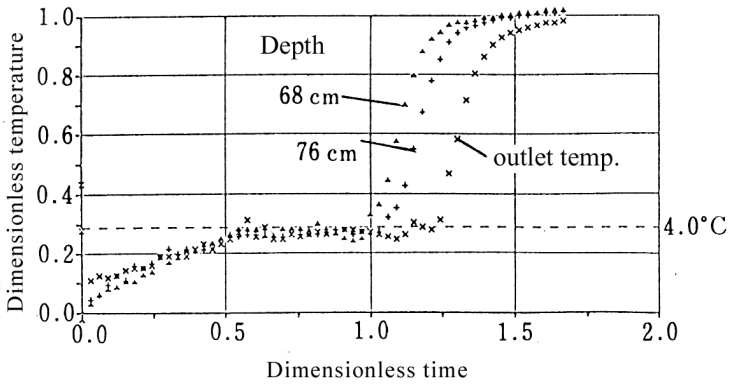

Fig. 9. Melting process for large Archimedes number and moderate inlet enthalpy flow rate

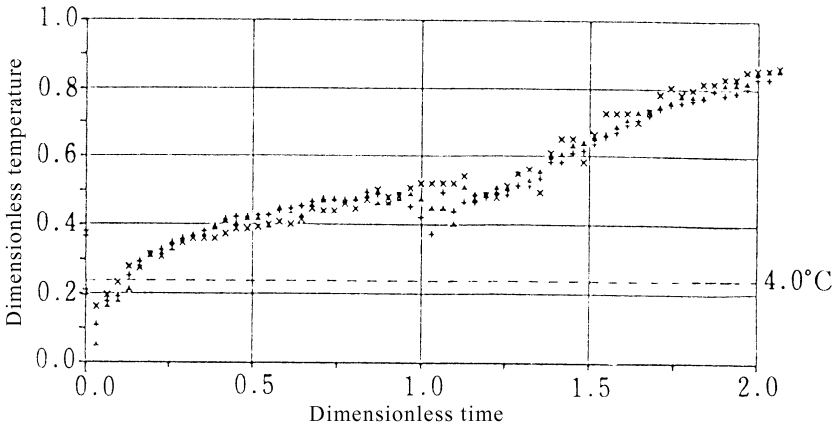

Fig. 10. Melting process for small Archimedes number

2.5 Effect of main parameters on efficiencies

The relationship among efficiency, Archimedes number, and inlet enthalpy flow rate is analyzed in this section. The efficiency depends on the limit temperature to the coils of the air handling units. Even though the value of the limit temperature depends on the design conditions of the air handling units, in the present study, the limit temperature was set to 4°C based on the above results. Figure 11 shows the relationship among η, Archimedes number, and inlet enthalpy flow rate. The effect on outlet response is more pronounced for the Archimedes number than for the enthalpy flow rate. This means that larger Archimedes numbers produce lower outlet temperatures. Figure 12 shows the relationship among η_0, Archimedes number, and inlet enthalpy flow rate. In this case, the enthalpy flow rate has more influence on the response than in the case of η.

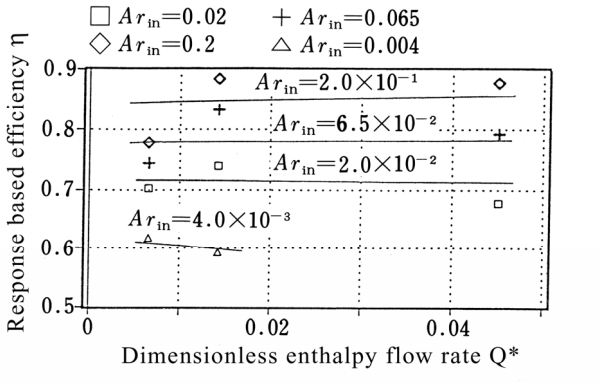

Fig. 11. Relationship between response-based efficiency η and inlet conditions

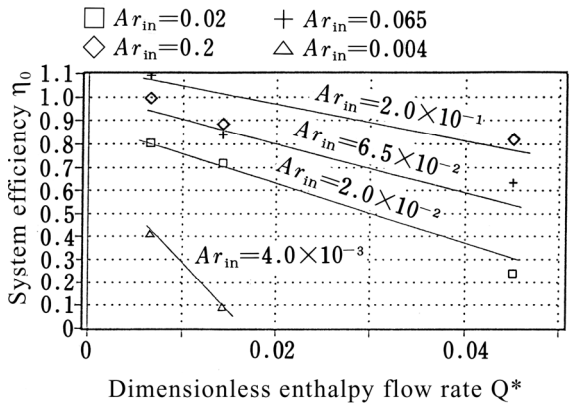

Fig. 12. Relationship between system efficiency η_0 and inlet conditions

2.6 Thermal response of the slurry ice storage tank

The dynamic ice making method, which makes ice using an additional device, is an alternative to the ice-on-coil ice storage tank. Since ice is intermittently or continuously removed from the surface of an ice making heat exchanger, no thermal resistance occurs, as in the case of the ice-on-coil ice storage tank. There are several types of dynamic ice making processes, which use a diluted glycol solution or the sub-cooling phenomenon of water. In the present paper, experiments were conducted on a dynamic ice storage tank using sub-cooled water.

2.6.1 Experimental setup and conditions

The experimental setup is shown in Figure 13 and includes a sub-cooling heat exchanger, which cools water to 2°C below the freezing point. The sub-cooled water was injected into the tank and collided with a plate at which the sub-cooled state was released.

The flow rates of the glycol solution and the input water for melting were measured by electromagnetic flow meters. Temperature profiles from 10 vertical points at two locations, as well as the inlet and outlet temperatures, were measured. Melting was performed by spray nozzles at the upper part of the tank.

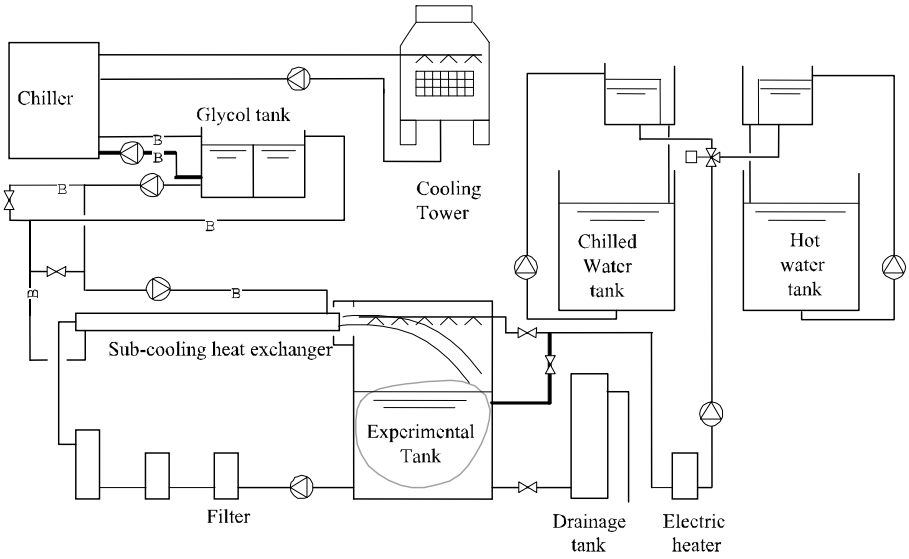

Fig. 13. Schematic diagram of the experimental setup for slurry ice storage

Exp. no.	Initial temp. [°C]	Charging time [hr:min]	IPF [%]
SD101C	15.8	4:30	43.9
SD102C	19.6	4:35	17.4
SD103C	16.4	4:20	58
SD104C	14.4	------	27.2
SD105C	11.7	4:30	44.6
SD106C	15.6	4:55	44.3
SD107C	13.0	4:40	34.4
SD108C	5.3	3:50	33.9
SD109C	16.1	4:40	45.8
SD110C	13.5	4:10	30.5
SD111C	16.8	4:05	31.9
SD112C	14.5	4:10	31.8

Table 5. Experimental conditions for the freezing process for the slurry ice storage tank

Exp. no.	Inlet temp. [°C]	Flow rate [l/min]	Inlet heat [kW]
SD101H	38.5	12.6	33.8
SD102H	29.7	16.1	33.4
SD103H	24.8	19.4	33.6
SD104H	17.5	27.3	33.3
SD105H	29.7	11.1	23.0
SD106H	24.6	12.9	22.1
SD107H	17.1	19.8	23.6
SD108H	13	24.9	22.6
SD109H	18	8.7	10.9
SD110H	12.3	10.6	9.1
SD111H	12.6	12.2	10.2
SD112H	9.9	15.7	10.8

Table 6. Experimental conditions for the freezing process for the slurry ice storage tank

2.7 Results

Figure 14 shows the temperature variation of the tank and the glycol solution during a freezing process. Since sub-cooled water was injected from the heat exchanger into the tank, the inside of the tank was completely mixed so that the temperature profile was uniform. The temperature of the tank decreased from the beginning of the experiment and reached 0°C after two hours. Once the inside of the tank reached the freezing temperature, heat extraction from the heat exchanger was used to form ice. Therefore, the temperature of the glycol solution was maintained at approximately 4°C below the freezing point.

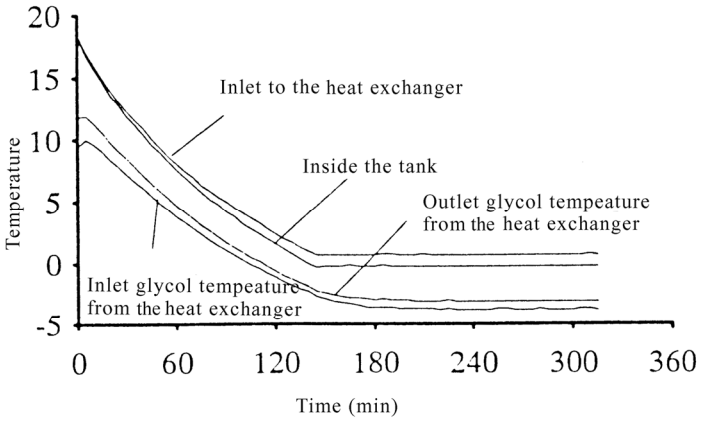

Fig. 14. Freezing process of the slurry ice storage tank

The injected water was released from its sub-cooled state by the collision, and 2% of the water was frozen. Ice in the shape of tiny flakes was observed to float inside the tank. There was no constraint on ice formation, which was different from that in the ice-on-coil ice storage tank. After a certain amount of ice flakes was produced, a lump of ice formed by agglomeration of the ice flakes. Experiments to examine the freezing process were continued until the lump of ice extended to the bottom of the tank. The value of the IPF was calculated from the heat balance between the extracted heat by the glycol solution and the sensible and latent heat of water inside the tank. The IPF reached a higher value than that for the ice-on-coil ice storage tank, in which the thickness of the ice was limited by the space between the ice making coils.

Dimensionless output responses of melting processes are shown in Figures 15 and 16. Since the temperature at the maximum density of water, i.e., 4°C, is also important for the slurry ice type, the points at which the outlet temperature exceeded 4°C are indicated by filled circles in the figures. The outlet temperature was maintained at temperature lower than 4°C from the beginning of the experiments and increased to dimensionless temperatures of 0.7 to 1.0. The response shape indicated complete mixing and a lack of significant difference between experimental conditions. The dimensionless time, when the response increased, appeared earlier for larger inlet enthalpy flow rates.

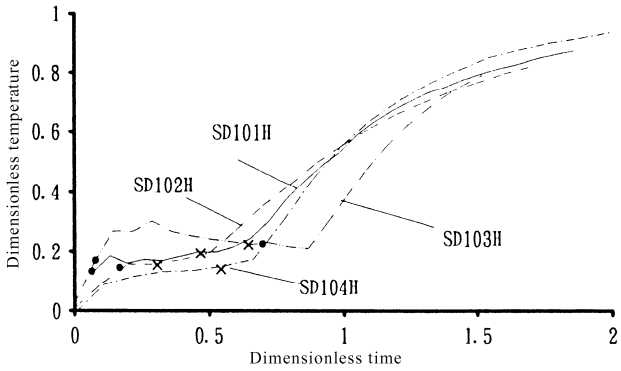

Fig. 15. Dimensionless response of the melting process for slurry ice storage for large inlet enthalpy flow rate

Considering the time at which the outlet temperature exceeded 4°C, the real temperature before response increase differed for different inlet conditions. The temperature exceeded 4°C at a dimensionless time of approximately 0.1 for certain conditions. However, the temperature remained above 4°C until a dimensionless time of approximately 0.8 for other conditions. The dimensionless times at which the inlet enthalpy became equal to the latent heat of the ice are indicated in the figures by cross symbols. As observed from the figures, the temperature had already increased when ice remained present in the tank.

The time at which the outlet temperature exceeded 4°C is considered to depend on the relationship between the enthalpy flow rate and the heat transfer to the ice. The ice in the slurry ice tank was in the form of particles and was distributed over the entire tank. Therefore, heat transfer occurred over a larger area than for the ice-on-coil ice storage tank, and depended strongly on the state of mixing inside the tank. As the Archimedes number

became small, which indicates a higher velocity at the inlet, mixing inside the tank was accelerated and so the heat transfer between ice and water was enhanced. Consequently, the outlet temperature remained lower for small Archimedes numbers.

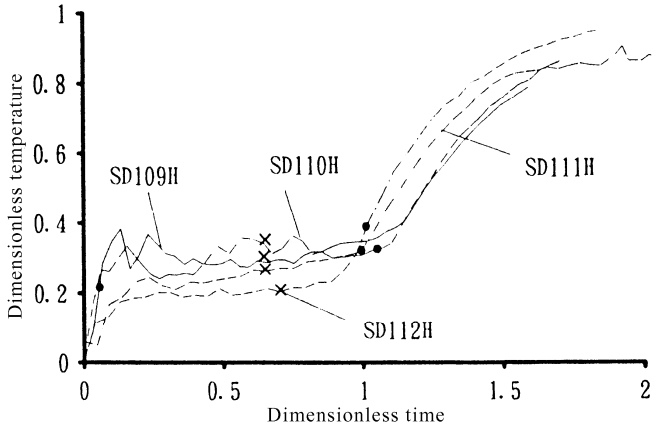

Fig. 16. Dimensionless response of the melting process of slurry ice storage for small inlet enthalpy flow rate

The temperature of the outlet flow and its duration below 4°C are important for system utilization. The efficiency defined by the dimensionless response was difficult to apply to slurry ice storage, because the outlet temperature sometimes exceeded 4°C. Therefore, the relationship between efficiencies and experimental conditions is not discussed for the case of slurry ice storage.

3. Evaluation of a PCM storage system using paraffin waxes

Phase change materials other than ice and water have been extensively investigated as a TES medium. In recent years, various commercially available materials have been developed. Research on the use of PCMs in buildings have been conducted. The thermal characteristics of building materials with PCMs, which could stabilize the temperature of a room, were measured (Mehling, 2002). Organic compounds, such as fatty acids and paraffin waxes, have also attracted attention as TES media. The melting temperature of a binary mixture of these materials is adjustable to climate requirements (Kauranen et al. 1991). The heats of fusion of these materials were from 120 to 160 kJ/kg (Feldman et al. 1989). Both heating and cooling applications are attractive for use with binary mixtures of tetradecane and hexadecane (He et al. 1999).

Several studies on building materials containing PCM have been conducted. Gypsum boards combined with a mixture of fatty acids could reduce the fluctuation of room temperature in the wintertime (Shilei et al. 2006). Floor panels mixed with PCM in an under-floor electrical heating system were evaluated because of the availability of inexpensive electricity during the nighttime (Lin et al. 2003). Applications of PCMs to ceilings and wallboards, which were cooled during the nighttime and released stored energy for cooling during the day, were examined (Barnard and Setterwall 2003, Lin et al. 2003 and Feldman et

al. 1995). These studies focused on the use of natural heat resources in conjunction with TES technologies.

On the other hand, TES is commonly used in warm countries, because the electric peak demand may be problematic. In such countries, electric consumption of heating, ventilating, and air conditioning (HVAC) systems is concentrated during warm summer afternoons. Therefore, the demand for electricity has a steep peak. This peak should be shaved to off-peak hours in order to avoid electricity shortages. Water and ice storage can be used for this purpose. Ice storage has become common, because the volume of the storage tank is smaller than water storage tank due to the latent heat of water. However, chilling machines are less efficient than ordinary machines used for comfort cooling. The use of a PCM having a higher melting temperature than ice is promising because the operating temperature need not be changed from ordinary operation.

Phase change material storage devices can be installed in the water circuit or the air circuit of HVAC systems. Since the temperature difference between the PCM and the heat transfer medium is needed in order to solidify or liquefy, an air circuit with a wide temperature range was considered to be suitable. We proposed a system with PCM containers in the air ducts. The materials selected in the present study were mixtures of various paraffin waxes, which allowed the melting temperature to be adjusted by adjusting the concentration of each material. Simple methods by which to determine the thermal properties of the PCM were proposed by comparing the temperature response of the PCM samples with water (Zheng et al. 1999 and Martin et al. 2003). In the present study, the thermal characteristics of the mixtures were measured using a simple apparatus and simulations of an HVAC system were conducted in order to evaluate various properties, such as the melting temperature or the quantity of the mixture. The performance of the proposed system was evaluated using a system simulation program.

3.1 Research methods

The melting temperature can be changed by adjusting the concentrations of paraffin waxes (He et al. 1999). We used industrial grade paraffin waxes. Table 7 lists the concentrations of the mixtures. The use of flammable liquids at 20°C in buildings is prohibited by Japanese building codes. A fatty acid, namely, stearic acid with a high melting temperature, was added to solidify the mixture of paraffin waxes. The apparatus shown in Figure 17 was used to measure the thermal properties of the mixtures. The apparatus consisted of foam polystyrene covered with acrylic plates. A cavity was located in the center of the apparatus, which was filled with the mixture. The surface areas of the cavity were covered with heat flux transducers. Thermocouples were placed inside the cavity.

	Estimated melting temp.	Concentration of paraffin wax (t_m: 18°C)	Concentration of paraffin wax (t_m: 28°C)	Concentration of stearic acid	Mass of PCM (g)
MT 17	17°C (62.6°F)	40%	40%	20%	39.1
MT 19	19°C (66.2°F)	28%	52%	20%	40.4
MT 21	21°C (69.8°F)	24%	56%	20%	40.0
MT 23	23°C (73.4°F)	16%	64%	20%	38.5

Table 7. Concentrations of paraffin waxes and fatty acid used in the present study
t_m: melting temperature

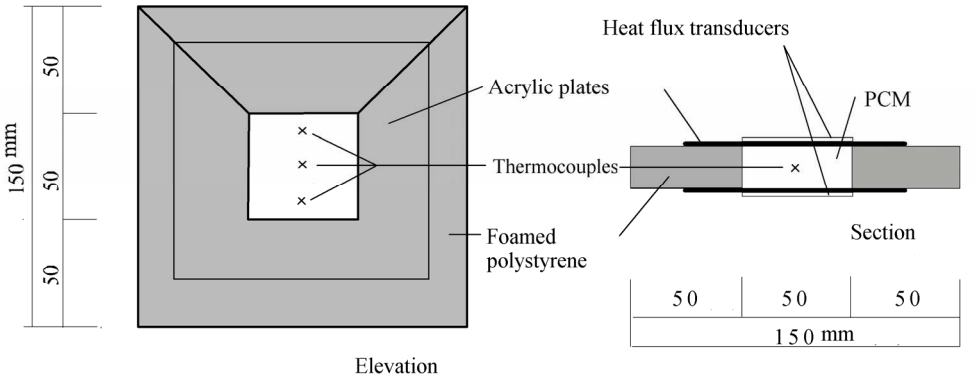

Fig. 17. Experimental apparatus used to measure the thermal properties of the mixtures

The apparatus was placed in a small thermal chamber in which both temperature and humidity could be controlled. The temperature inside the chamber was raised from –5°C to 30°C over seven hours. The temperature inside the chamber was maintained at 30°C for three hours and decreased to –5°C over seven hours, before being maintained constant for seven hours. One cycle of the experiment was continued over 24 hours, and seven cycles were repeated for each measurement. The first and last cycles were not used for analysis because of the instability of the experimental conditions.

3.2 Results

The results for the MT17 mixture are shown in Figure 18. The left-hand figure shows the sum of the heat through the heat flux transducers versus the average temperature of the thermocouples for five cycles. The specific heat could be obtained by differentiating the curve as is shown on the right-hand side of the figure. The measured enthalpy was integrated as latent heat in the temperature range for the phase change observed in Figure 2(b), where the temperature ranged from 11.5°C to 20.5°C for freezing and from 10.0°C to 21.5°C for melting. The results for all of the mixtures are listed in Table 2. The latent heat of

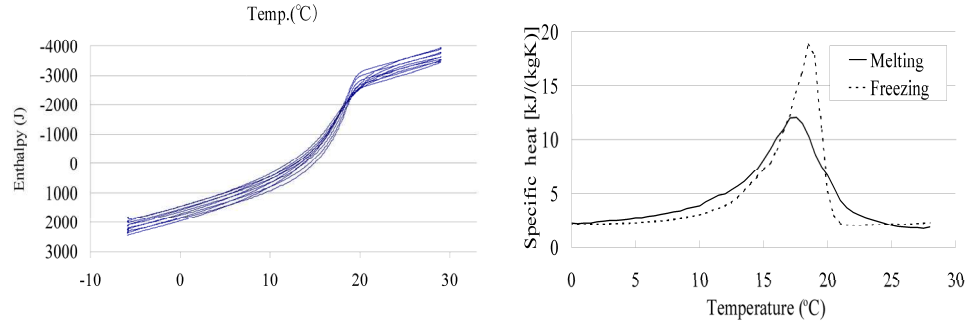

(a) (b)

Fig. 18. Results for the MT17 mixture

pure paraffin wax is approximately 200 kJ/kg. The mixtures had smaller latent heats than the pure material. The measured latent heat was equivalent to the heat for a temperature difference of 20°C for water.

The curves shown in Figure 18(b) were used for simulations, which used the enthalpy method of the PCM. In the simulation program, the specific heat of the materials varied with temperature according to the curves shown in the figure (Yamaha et al. 2001).

Materials	Operations	Peak temperature [°C]	Amount of latent heat [kJ/kg]
MT 17	Freezing	18.5	86
	Melting	17.5	77
MT 19	Freezing	21.5	87
	Melting	20.5	86
MT 21	Freezing	21.5	85
	Melting	20.5	87
MT 23	Freezing	21.5	76
	Melting	22.0	83

Table 8. Thermal properties of materials

3.3 System simulations

The use of the mixtures was evaluated through computer simulations. The section and plan of the building used in the simulations are shown in Figure 19, and a schematic diagram of the system is shown in Figure 20. An air conditioning system for an office building was assumed. The calculated area was part of one floor of an office building with a floor area of 73.8 m² that was assumed to be located in Nagoya City, Japan. The room had windows of 6.5 m² facing south, and the weather data used to calculate the peak load was the data for a summer day. The wall was constructed using lightweight concrete and was insulated with 25-mm-thick foam urethane.

For charging operation, the air runs through the closed circuit of the PCM storage tank and the air conditioner (Figure 20, (1)). After the end of the charging cycle, the ordinary air conditioning operation was started. The conditioned air is projected into the room and returned to the air conditioner after mixing with a volume of outdoor air. In this operation, the air is assumed to bypass the PCM storage tank (Figure 20, (2)). For the discharging operation, the air passes into the room through the PCM storage tank. In the charging and discharging operations, the airflow rate is reduced to half that of the ordinary air conditioning in order to store and recover heat effectively (Figure 20, (3)). The discharging period started at 13:00 and ended at 16:00. In Japan, utility companies offer special discount rates for peak shaving during this period.

Calculation was conducted using the enthalpy method, which assumed the heat of fusion of PCM to be a specific heat $c_p(\theta)$ that varied with temperature. The temperature of the PCM was calculated by combining the experimental results shown in Figure 2 with the one-dimensional heat conduction equation:

$$\frac{\partial}{\partial t}\left[\rho c_p(\theta)\theta_p\right] = \frac{\partial}{\partial x}\left(\lambda_p \frac{\partial \theta_p}{\partial x}\right) + \frac{S}{dz_p} \tag{12}$$

where S is heat flux through the PCM capsule wall, which is calculated as follows:

$$S = \frac{1}{1/h + 1/\lambda_c}\left(\theta_a - \theta_p\right) \tag{13}$$

The heat from the PCM to the circulating air was calculated by heat convection on the surface of the PCM containers. The convection coefficient was calculated using the following empirical equation for a flat surface (Incorpera et al. 1996):

$$Nu = 0.037\,\mathrm{Re}^{0.8}\,\mathrm{Pr}^{1/3} \tag{14}$$

The heat transfer between a container of PCM and air in the duct was enhanced by fins extended toward the air. The fins increased the surface 18.2 times as compared to a flat surface. The heat balance among the air entering the room, the heat transfer from outdoor air, and the internal heat gain determined the temperature of room is as follows:

$$c_r \frac{d\theta_r}{dt} = UA\left(\theta_o - \theta_r\right) + V\left(\theta_i - \theta_r\right) \tag{15}$$

Charging was conducted for three hours, from 5:00 to 8:00, followed by ordinary air conditioning from 9:00. Discharging started at 13:00 and ended at 16:00. The charging hours were set to be equal to the discharging hours. The inlet temperature to the PCM storage tank for the charging operation was 12°C, and the inlet temperature to the room (θ_i) during ordinary air conditioning was 16°C. No temperature control was performed during the discharging operation. During the ordinary air conditioning, the air flow rate to the room was controlled in order to maintain the temperature of the room at 26°C. The mixture quantities were 50, 100, 150, 200, 250, 300, 350, and 400 kg.

The room temperature was set to 25°C, as calculated by solving the heat balance for the heat transfer through walls and windows, internal heat, and release of stored cooling from the PCM. The calculation was conducted for two days for each condition. The results shown herein are the results for the second day.

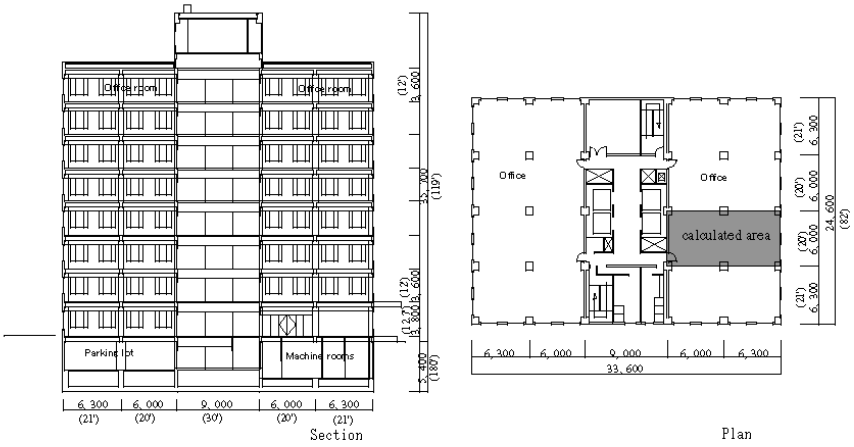

Fig. 19. Section and plan of the building used for simulation

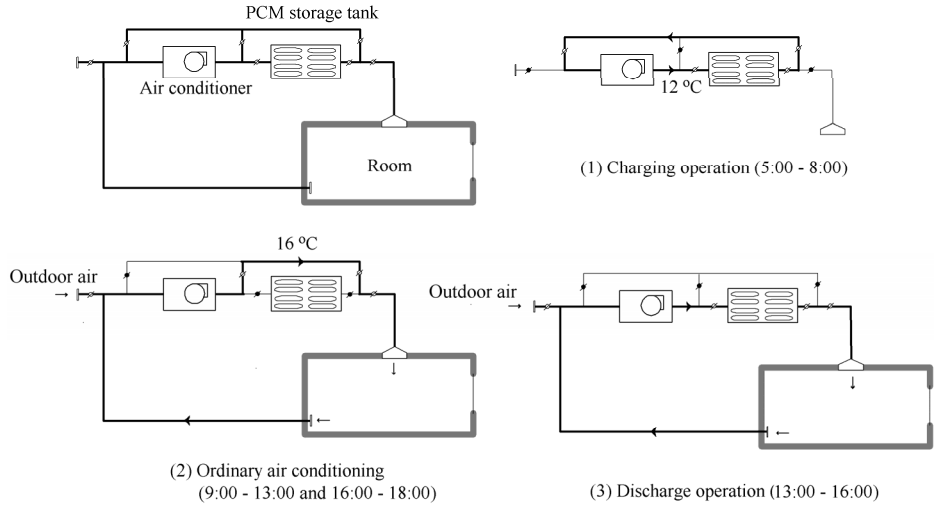

Fig. 20. Schematic diagrams of the HVAC systems used in the simulations

The results are shown in Figure 21 for 100 and 400 kg of PCM. In the left-hand figure, the PCM mixture was cooled to air temperature (12°C) as soon as the charging operation started. During the discharging operation, the stored heat was not large enough to maintain the room temperature. Consequently, the room temperature was raised to 35°C. The right-hand figure shows the results for 400 kg. The temperature during charging and discharging operations decreased gradually due to latent heat. The stored heat had sufficient capacity to maintain the room temperature near the set point.

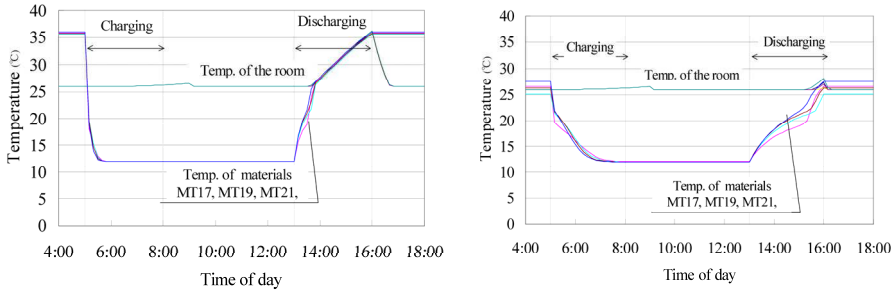

Fig. 21. Comparison of temperature fluctuation using 100 kg or 400 kg of PCM

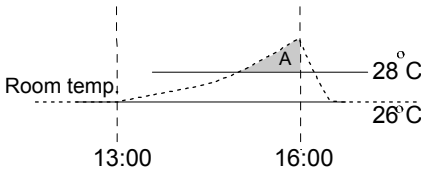

Fig. 22. Index used to evaluate the investigated effect

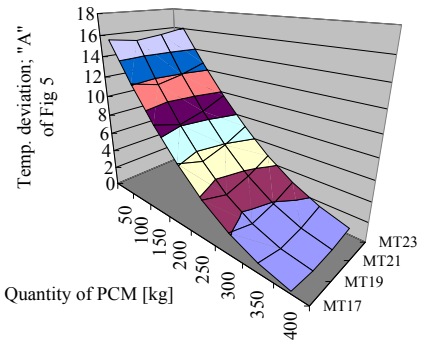

Fig. 23. Relationship among the index, the materials, and the quantities

3.4 Discussion

The purpose of this system was to control the temperature increase while the refrigeration machines were stopped. The evaluation of the system focused on the degree to which the temperature fluctuated. Assuming that 28°C is the allowed indoor temperature, the area A shown in Figure 22, which is the difference between the room temperature and 28°C, was used as an index of temperature deviation. This index increases as the temperature in the room increases.

Figure 23 shows the relationship between the index, the quantity of PCM, and the PCM mixture. The temperature deviation decreased as the quantity of PCM mixture increased. The index or the temperature deviation was very small for 400 kg of PCM, which was equivalent to 5.4 kg/m² of PCM. The differences among the various materials were not significant. The index was larger for materials with higher melting temperatures (MT23, MT21). Because of its lower melting temperature, the most effective material was MT19. Moreover, MT 17 melted too quickly.

In the system discussed in the present paper, the PCM would be maintained in containers and installed in air ducts. The heat transfer between the surface of the container and the air in the duct would be a significant problem. Since thermal conductivities of paraffin waxes are small, the material would not be sufficiently melted or frozen, unless some enhancements, such as fins, were adopted. Although, in the present study, fins were adopted, for real applications, the structure of the container should be simple in order to decrease the cost of construction.

In the present study, there was no consideration of the humidity because the program only treated the heat transfer problem. The humidity has a large influence on thermal comfort. The dew point of 26°C and RH 50% air is lower than 17°C, so the humidity of the room would increase during the discharging operation. The humidity should be calculated because the sensible heat load is relatively small in an office building.

4. Conclusions

Thermal energy storage systems are used to shift peak heat load to off-peak hours. The performance depends on the design and installation of such systems. The performances of two types of TES, which use ice and paraffin waxes, were analyzed. Ice storage systems

were analyzed as HVAC system components, and a storage system using paraffin waxes was evaluated for use by a passive method.

Ice-on-coil and slurry ice storage system were considered. Several definitions of efficiency as indices of evaluation were discussed. The temperature response of an ice-on-coil storage system depends on the mixing condition. Large Archimedes numbers at the inlet result in a longer duration of low outlet temperature. The effects of the operating conditions on the energy and response-based efficiencies were also examined. The response-based efficiency was more sensible to the normalized inlet enthalpy flow rate. For the slurry ice storage tank, the time at which the outlet temperature reached 4°C varied according to experimental conditions. Since the ice in the slurry ice tank consisted of tiny floating particles, the higher velocity could enhance heat transfer and result in lower outlet temperatures

For storage system using paraffin waxes, an air distribution system with the PCM tank in the air ducts was proposed. The system was used for cooling and could take advantage of discounted electricity rates at night. The materials that could be used in the system, were obtained by mixing paraffin waxes and fatty acids. The thermal properties of the materials were measured. The melting temperature could be controlled by adjusting the concentration of each material, although the latent heat of the measured mixtures was less than that of the pure paraffin wax.

The system performance was examined through a computer simulation, and the necessary quantity of material was evaluated. The PCM was cooled from 5:00 to 8:00 am using discounted electricity. The stored heat was discharged from 13:00 to 16:00, when the peak load of cooling occurred. As the refrigeration machines were stopped during this period, the temperature of the room fluctuated. The temperature deviation was taken as an index, and the system was evaluated. For an ordinary office building in Nagoya City, which is located in the same climate as major cities with more than two million inhabitants in Japan, 400 kg of PCM for 73.8 m² of room surface (or 5.4 kg/m² of PCM) could maintain the room temperature to be constant without any cold source operation. The melting temperature suitable for the system was approximately 19°C, which could be achieved using MT19.

5. Nomenclature

A : wall surface area
Ar_{in} : Archimedes number at the inlet
c : specific heat
d_{in} : diameter of the inlet of the tank
dz : thickness of PCM
g : gravitational acceleration
h: convective coefficient
H_t : heat removed from a storage tank
H_{tc} : heat removed until the outlet temperature reaches the limit temperature
IPF : (Ice Packing Factor) ratio of ice volume to tank volume (= V_{ice}/V_0)
L : heat of fusion of water
Nu : Nusselt number
Pr : Prandtl number
q : heat flow from coil
Q^*: dimensionless enthalpy flow rate
Q : flow rate of inlet water

Re : Reynolds number
T, t : time
Tc : limit temperature to the coils of the air handling units
u_{in}: velocity of inlet water
u: velocity of water inside the tank
U : average overall heat transfer coefficient
V : airflow rate to the room
V_0 : volume of tank
V_{ice} : volume of ice
x : length in the flow direction,
η : response-based efficiency
η_0 : system efficiency
η_v : volumetric efficiency
θ_0 : initial temperature
θ_{in} : temperature of the inlet water
θ_{out} : temperature of the outlet water
θ_c : limit temperature to the coils of the air handling units
$\Delta\theta_i$: equivalent temperature difference for ice storage (= L • IPF/c)
$\Delta\theta_0$: temperature difference of the coils of the air handling units
ρ : density of inlet water
ρ_0 : density of water at the initial temperature
ρ_{ice} : density of ice
$\Delta\rho$: density difference between the inlet water to the tank and the initial temperature of water in the tank
λ : thermal conductivity
θ_a : temperature of air
θ_p : temperature of PCM
θ_r : temperature of the room
* indicates a dimensionless value

6. References

Barnard, N and Setterwall, F, (2003), Thermal Mass and Night Ventilation - Utilising "hidden" Thermal Mass, *Proceedings of Workshop IEA Annex 17*, Indore. Mar. 2003.

Feldman, D, Shapirom, M M, Banu, D and Fuks, C J, (1989), Fatty Acids and Their Mixtures as Phase-Change Materials for Thermal Energy Storage. *Solar Energy Material,* Vol. 18, Issue 3-4, pp. 201-216. ISSN 0927-0248

Feldman, D, Banu, D, and Hawes, D W, (1995), Development and Application of Organic Phase Change Mixtures in Thermal Storage Gypsum Wallboard, *Solar Energy Materials and Solar Cells,* Vol. 36, Issue 2, pp. 147-157. ISSN 0927-0248

He, B, Gustafsson, M, and Setterwall, F, (1999), Tetradecane and Hexadecane Binary Mixtures as Phase Change Materials (Pcms) for Cool Storage in District Cooling Systems. *Journal of Energy*, Vol. 24, Issue 12, 1015-1028. ISSN: 0360-5442

Incropera, F and DeWitt, D, (1996), *Fundamentals of Heat and Mass Transfer,* John Wiley & Sons., ISBN 0-471-30460-3, New York

Kauranen, P, Peippo, K, and Lund, P D, (1991), An Organic PCM Storage System with Adjustable Melting Temperature. *Solar Energy,* Vol. 46, Issue 5, pp. 275-278. ISSN: 0038-092X

Lin, K, Zhang, Y, and Jiang, Y, (2003), Simulation and Evaluation of the Thermal Performance of PCM Wallboard Rooms Located in Different Climate Regions of China in Summer, *Proceedings of the ASME/JSME Thermal Engineering Joint Conference:* 71, Hawaii, Mar. 2003

Mehling, H, (2002), News on the Application of PCMs for Heating and Cooling of Buildings. *Proceedings of Workshop IEA Annex 17,* Tokyo, Sept. 2002.

Shilei, L, Neng, Z, and Gouhui, F, (2006), Impact of Phase Change Wall Room on Indoor Thermal Environment in Winter. *Energy and Buildings*, Vol. 38: 18-24.

Tamblyn, R T, (1977), Thermal storage: it saves and saves and saves. *ASHRAE Transaction* Vol. 83, Part 1, pp.677-684, ISSN: 0001-2505

Yamaha, M, Shuku, K, and Misaki, S, (2001), A Study on Thermal Characteristics of Thermal Storage Tank Using Phase Change Material Installed in an Air Distribution System, *Transaction of AIJ.* No. 549, pp. 51-57. ISSN 1348-0685.

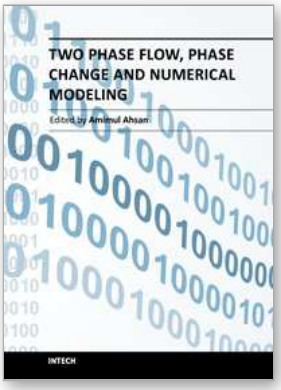

Two Phase Flow, Phase Change and Numerical Modeling

Edited by Dr. Amimul Ahsan

ISBN 978-953-307-584-6
Hard cover, 584 pages
Publisher InTech
Published online 26, September, 2011
Published in print edition September, 2011

The heat transfer and analysis on laser beam, evaporator coils, shell-and-tube condenser, two phase flow, nanofluids, complex fluids, and on phase change are significant issues in a design of wide range of industrial processes and devices. This book includes 25 advanced and revised contributions, and it covers mainly (1) numerical modeling of heat transfer, (2) two phase flow, (3) nanofluids, and (4) phase change. The first section introduces numerical modeling of heat transfer on particles in binary gas-solid fluidization bed, solidification phenomena, thermal approaches to laser damage, and temperature and velocity distribution. The second section covers density wave instability phenomena, gas and spray-water quenching, spray cooling, wettability effect, liquid film thickness, and thermosyphon loop. The third section includes nanofluids for heat transfer, nanofluids in minichannels, potential and engineering strategies on nanofluids, and heat transfer at nanoscale. The forth section presents time-dependent melting and deformation processes of phase change material (PCM), thermal energy storage tanks using PCM, phase change in deep CO2 injector, and thermal storage device of solar hot water system. The advanced idea and information described here will be fruitful for the readers to find a sustainable solution in an industrialized society.

How to reference

In order to correctly reference this scholarly work, feel free to copy and paste the following:

Motoi Yamaha and Nobuo Nakahara (2011). Thermal Energy Storage Tanks Using Phase Change Material (PCM) in HVAC Systems, Two Phase Flow, Phase Change and Numerical Modeling, Dr. Amimul Ahsan (Ed.), ISBN: 978-953-307-584-6, InTech, Available from: http://www.intechopen.com/books/two-phase-flow-phase-change-and-numerical-modeling/thermal-energy-storage-tanks-using-phase-change-material-pcm-in-hvac-systems

INTECH
open science | open minds

InTech Europe
University Campus STeP Ri
Slavka Krautzeka 83/A
51000 Rijeka, Croatia
Phone: +385 (51) 770 447
Fax: +385 (51) 686 166
www.intechopen.com

InTech China
Unit 405, Office Block, Hotel Equatorial Shanghai
No.65, Yan An Road (West), Shanghai, 200040, China
中国上海市延安西路65号上海国际贵都大饭店办公楼405单元
Phone: +86-21-62489820
Fax: +86-21-62489821